フッ化物リン酸塩ガラスの光学特性と局所構造に対するO/P比の寄与

吉本幸平，上田　基，山本優也，水口雅史

Impact of the O/P Ratio on the Optical Properties and Structures of Fluoride–Phosphate Glass†

Kohei YOSHIMOTO, Motoi UEDA, Yuya YAMAMOTO and Masafumi MIZUGUCHI

フッ化物リン酸塩ガラスは，低屈折率・低分散，良好な紫外域透過率，正の異常分散など特異な光学特性を有することから光学材料として多用されている．しかし，その組成の複雑さのためか，光学特性や構造の組成依存性に関する系統的な知見は少ない．本研究では，$Ca(PO_3)_2$–AlF_3–CaF_2–BaF_2–BaO系フッ化物リン酸塩ガラスを溶融急冷法により作製し，その光学特性や構造の組成依存性をO/P比に着目して評価した．結果，ガラスの光学特性や局所構造が，O/P比に対して非線形的な挙動を示すことが明らかとなった．例えば，O/P=3.0–3.4におけるバンドギャップエネルギーは概ね一定であるが，O/P比が3.6から4.0にかけて急激な低下を示した．また，Lorentzモデルに基づく屈折率分散の解析から，バンドギャップエネルギーと同様に紫外域の共鳴周波数もO/P=3.6–4.0において急激に低下することが明らかになった．さらに，赤外吸収分光法およびラマン散乱分光法によるガラスの局所構造解析から，O/P比が3.6から4.0にかけて，リン酸鎖の切断や孤立Q^0構造の増加など，劇的な構造変化が生じることも示唆された．前記光学特性と局所構造の特徴的なO/P比依存性を包括するメカニズムを示すため，電気陰性度や光学的塩基度の考え方を活用して原子間の化学結合状態に基づく考察を行った．

$Ca(PO_3)_2$–AlF_3–CaF_2–BaF_2–BaO glasses were prepared by the melt quenching method, and the effects of the O/P ratio on the optical properties and glass structure were investigated. The bandgap energy showed no significant change at O/P = 3.0–3.4 but drastically decreased with the increase in the O/P from 3.6 to 4.0. In addition, the refractive index dispersion was analyzed based on the Lorentz model, and it was found that the decrease in the resonance frequency in the ultraviolet region with the increase in the O/P ratio resulted in an increase in the refractive index and dispersion. Analysis of the infrared absorption and Raman scattering spectra revealed that the phosphate chains were broken, and isolated Q^0 units were generated with the increase in the O/P ratio from 3.6 to 4.0. Based on the structural change of the glass, the origin of the nonlinear dependence of the optical properties on the O/P ratio was discussed.

Key words フッ素化合物，ガラス，光学材料／光学特性，リン酸，構造
fluorine/fluorine compounds, glass, optical materials/properties, phosphates, structure

1 Introduction

Fluoride–phosphate glass is widely used as an optical material owing to its unique optical properties, such as high optical transmittance in the ultraviolet (UV) to infrared (IR) range, low refractive index dispersion, and positive anomalous partial dispersion, which are not obtained with oxide glasses [1]–[4]. Although fluoride is not a typical glass-forming system, the addition of a small amount of phosphate dramatically improves its glass-forming ability and thermal and chemical stabilities while maintaining the unique optical properties resulting from the highly ionic cation–fluorine bonds. Owing to its excellent optical properties, the fluoride–phosphate system was commercially melted as optical glass at Schott in the 1960s [5], and many studies have since been conducted on the structure and physical properties of fluoride–phosphate glasses [1]–[4], [6]–[13]. Phosphorus oxide, which is a glass-forming oxide, plays an important role in constructing the glass network in fluoride–phosphate glass. It has been established that the phosphate units in phosphate glass exhibit various structures depending on the O/P ratio, such as networking ultraphosphate, Q^3 (O/P =

† This paper is reprinted with permission from John Wiley and Sons of reference [34]. We acknowledge John Wiley and Sons for the permission.

2.5), chain-like metaphosphate, Q^2 (O/P = 3.0), dimer-like pyrophosphate, Q^1 (O/P = 3.5), and isolated orthophosphate, Q^0 (O/P = 4.0) [14], where Q^n denotes tetrahedral PO_4 unit with n bridging oxygens. To the best of our knowledge, however, most studies on fluoride–phosphate glasses have focused on the metaphosphate (O/P = 3.0) composition, whereas very few studies have focused on the effects of the O/P ratio. In this study, we investigate the influence of the O/P ratio on the optical properties of fluoride–phosphate glasses and discuss the results based on the structural analysis of the glass.

2 Experimental Procedures

Fluoride–phosphate glasses were synthesized using an ordinal melt-quenching technique. The raw materials of $Ca(PO_3)_2$ (Rasa Industries, Ltd., Tokyo, Japan), AlF_3 (Morita Chemical Industries Co., Ltd., Osaka, Japan), CaF_2 (Hakushin Chemical Laboratory Co., Ltd., Tokyo, Japan), BaF_2 (Hakushin Chemical Laboratory Co., Ltd., Tokyo, Japan), and $BaCO_3$ (Nippon Chemical Industrial Co., Ltd., Tokyo, Japan) were weighed and mixed to obtain a glass weight of 100 g and then melted under the ambient atmosphere at 1223 K for 1 h in a platinum crucible. The glass compositions synthesized in this study are listed in Table 1. Hereinafter, the sample names of the $Ca(PO_3)_2$–AlF_3–CaF_2–BaF_2–BaO glasses are abbreviated as OP*X*, where *X* denotes the O/P ratio. A platinum lid was used during melting to prevent volatilization from the molten glass. After stirring and homogenization with a platinum propeller, the mixtures were poured into a steel mold, rapidly cooled, and immediately transferred to an annealing furnace maintained near the glass transition temperature, T_g. After holding at approximately T_g for 3 h, the glass was slowly cooled to room temperature at a rate of 16 K/h. The compositions of the glass samples were quantitatively analyzed by X-ray fluorescence (XRF) analysis, ZSX Primus II (Rigaku Corp., Tokyo, Japan). The impurities of the glass samples were quantitatively analyzed by inductively coupled plasma–mass spectrometry (ICP–MS), Agilent 7700 × (Agilent Technologies Inc., California, United States of America). For the ICP–MS analysis, the glass samples were dissolved by acid decomposition method. The crushed glass was placed in a platinum cell, and thermogravimetry-differential thermal analysis measurements, Thermo plus EVO2 TG8121 (Rigaku Corp., Tokyo, Japan), were performed at a heating rate of 10 K/min in the ambient atmosphere. The glass density was determined using the Archimedes method with deionized water as the immersion medium. For optical measurements, the glass was optically polished, and transmittance spectra were obtained in the range of 200–700 nm using a UV–Vis–NIR spectrophotometer, UH4150 (Hitachi High-Tech Science Corp., Tokyo, Japan), and in the range of 120–300 nm using a vacuum UV (VUV) spectrophotometer, KV-2004J (Bunkoukeiki Co., Ltd., Tokyo, Japan). The refractive index dispersion of the glass was measured using a Kalnew precision refractometer, KPR-3000 (Shimadzu Corp., Kyoto, Japan), at 11 wavelengths (i, h, g, F, e, d, C, r, and t lines and 1310 and 1550 nm). IR reflection spectra were measured using microscopic Fourier transform IR spectroscopy, Nicolet iN10 (Thermo Fisher Scientific Inc., Massachusetts, United states of America), in the range of 400–4000 cm^{-1} with reference to a gold mirror. The absorption spectra were obtained through the Kramers–Kronig transformation of the reflection spectra. Unpolarized Raman scattering spectra were measured at an excitation wavelength of 532.11 nm using a micro Raman spectrometer, NRS-5000 (JASCO Corp., Tokyo, Japan).

Table 1 Composition of OP*X* glasses

	$Ca(PO_3)_2$ (mol%)	CaF_2 (mol%)	BaF_2 (mol%)	BaO (mol%)	AlF_3 (mol%)	O/P
OP3.0	10	30	20	0	40	3.0
OP3.2	10	30	16	4	40	3.2
OP3.4	10	30	12	8	40	3.4
OP3.6	10	30	8	12	40	3.6
OP3.8	10	30	4	16	40	3.8
OP4.0	10	30	0	20	40	4.0

3 Results

Table 2 shows the results of an XRF analysis of OP*X* glass. The analyzed composition shows that almost linear correlation with the nominal composition, and no significant decrease in F occurred. The analyzed composition tends to be about 1 at% lower in cations and about 5 at% higher in oxygen than the nominal composition. However, similar trends were observed for Al_2O_3 (Nippon Light Metal Co., Ltd., Tokyo, Japan) and AlF_3 (Morita Chemical Industries Co., Ltd., Osaka, Japan) powders measured as standard samples, so these discrepancies between nominal and analyzed values are due to some systematic error in the measurements not due to the sample. Therefore, the results of XRF show that there were no serious compositional changes by the evaporation of fluorine.

Table 3 lists the thermal properties, densities, and optical properties of the OP*X* glasses. The increase in T_g with

Table 2　Results of the quantitative analysis of glass composition by X-ray fluorescence (XRF)

	Nominal composition						Analyzed composition					
	P (at%)	Al (at%)	Ca (at%)	Ba (at%)	O (at%)	F (at%)	P (at%)	Al (at%)	Ca (at%)	Ba (at%)	O (at%)	F (at%)
OP3.0	5.0	10.0	10.0	5.0	15.0	55.0	3.5	8.6	8.8	4.1	19.4	55.6
OP3.2	5.1	10.1	10.1	5.1	16.2	53.5	3.7	8.6	8.8	3.9	20.4	54.6
OP3.4	5.1	10.2	10.2	5.1	17.4	52.0	3.9	8.4	8.6	4.0	22.3	52.9
OP3.6	5.2	10.3	10.3	5.2	18.6	50.5	4.0	8.5	8.7	4.0	23.3	51.4
OP3.8	5.2	10.4	10.4	5.2	19.8	49.0	4.0	8.4	8.6	4.0	24.8	50.1
OP4.0	5.3	10.5	10.5	5.3	21.1	47.4	4.0	8.5	8.6	4.0	26.0	48.8
Al_2O_3		40.0			60.0			33.4			66.5	0.1
AlF_3		25.0				75.0		21.8			3.8	74.4

Table 3　Thermal and optical properties of OP*X* glasses

	T_g (K)	T_x (K)	ΔT (K)	ρ (g/cm^3)	E_g (eV)	n_d	ν_d
OP3.0	712	844	132	3.59	7.03	1.46381	89.2
OP3.2	716	834	118	3.57	7.06	1.46638	88.6
OP3.4	719	846	127	3.58	7.04	1.47072	87.5
OP3.6	733	863	130	3.60	6.96	1.47711	86.9
OP3.8	744	870	126	3.62	6.92	1.48436	85.7
OP4.0	746	871	125	3.64	6.77	1.48946	85.0

increasing O/P ratio is due to the decrease in fluorine content in the glass. In the case of fluoride ions of fluorophosphate glasses, only one cation is enough for charge compensation of terminal F, such as P–F bonds. In the case of oxide ions, however, at least two cations are required to compensate the negative charge of an oxide ion, except for P = O double bonds. Thus, electrostatic interactions among structural units, such as $P(O, F)_4$, $Al(O, F)_n$, and cations of Ca and Ba, are supposed to be stronger in oxygen-rich OP*X* glasses, resulting in higher viscosity and T_g. Similar to T_g, the crystallization onset temperature, T_x, also increases with an increase in the O/P ratio. ΔT (= $T_x - T_g$) is often considered a measure of the thermal stability of glass against crystallization [15], [16], but no significant dependence on the O/P ratio is observed. The glass density increases slightly with increasing O/P ratio.

Figure 1 shows the 10-mm-thick internal optical transmittance spectra of OP3.0 and OP4.0. There is no significant difference in the position of the absorption edge between OP3.0 and OP4.0; however, OP4.0 shows a lower transmittance at 300–400 nm than OP3.0. As can be seen in the inset of Fig. 1, the 80% transmission wavelength, λ_{80}, does not change significantly with the O/P ratio at O/P = 3.0–3.4, but it exhibits drastic redshifts with the O/P ratio at O/P = 3.6–4.0.

Figure 2 shows the optical absorption spectra of OP3.0 and OP4.0 in the VUV region. The large absorption below 170 nm is the intrinsic interband absorption of the glass, and the absorption edge of OP4.0 is located in a longer wavelength region than that of OP3.0. The bandgap energy, E_g, is estimated from the Tauc plot according to the following equation, and the results are listed in Table 3:

$$\alpha h\nu = A(h\nu - E_g)^2 \quad (1)$$

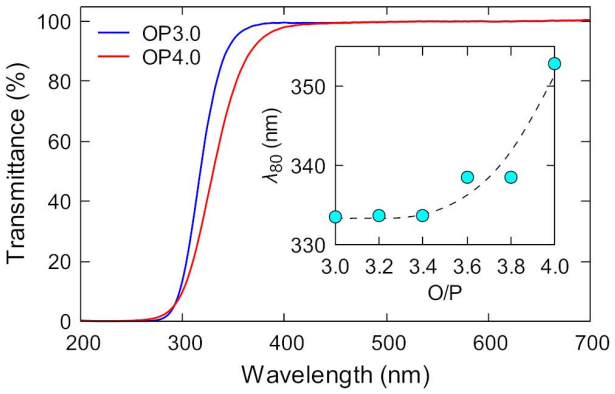

Fig. 1　Internal optical transmittance spectra (10 mm thick) of OP3.0 and OP4.0 glasses. The inset shows the O/P dependence of λ_{80}. The dashed line is shown to guide the eye.

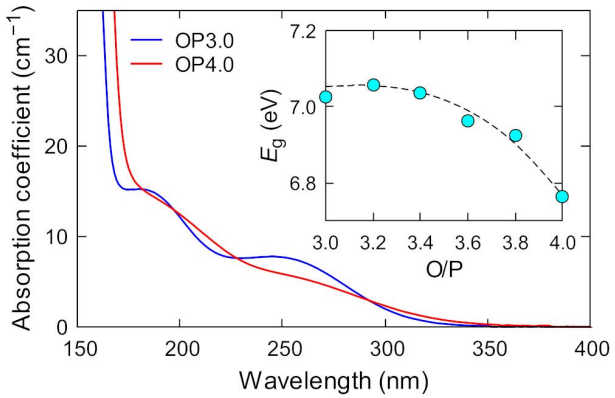

Fig. 2　Optical absorption spectra of OP3.0 and OP4.0 glasses in the vacuum ultraviolet (VUV) region. The inset shows the O/P dependence of E_g. The dashed line is shown to guide the eye.

where α, h, ν, and A are the absorption coefficient, Planck's constant, light frequency, and an energy-independent constant, respectively. The values of E_g for OP*X* glasses are close to those of other fluoride–phosphate glasses reported in the literature [4]. As shown in the inset of Fig. 2, E_g is almost constant at O/P = 3.0–3.4; however, at O/P = 3.6–4.0, it decreases rapidly as the O/P ratio increases.

Figure 3(a) shows the results of the spectral deconvolution of the absorption spectra of OP3.0 and OP4.0. The absorption spectra can be successfully reproduced with three Gaussian functions. The absorption near 180 and 260 nm is due to the charge-transfer state (CTS) of O 2p → Fe^{3+} 3d [2], [17], [18], where Fe ions are trace impurities present in the glass. Because the CTS is a parity-allowed transition, it has a large absorption coefficient, even at low concentrations of Fe^{3+} ions. Table 4 summarizes the results of the ICP–MS analysis of the OP*X* glasses. It can be seen that Fe is present as a trace impurity in the glass at a concentration of approximately 20 mg/kg in each sample, and the contents of other transition metals and Pt are significantly lower than that of Fe. Therefore, the effect of impurity elements other than Fe on the UV absorption is considered negligible.

The O/P dependence of the absorption peak positions near 180 and 260 nm is shown in Fig. 3(b). Neither peak position shows a significant change in the range of O/P = 3.0–3.4, but both peaks shift drastically toward lower wave numbers with an increase in the O/P ratio from 3.6 to 4.0. As shown in Fig. 3(a), the absorption in the region below 5 eV is dominated by the CTS of O 2p → Fe^{3+} 3d and is almost unaffected by the inherent absorption. Therefore, it is considered that the decrease in transmittance at 300–400 nm shown in Fig. 1 is due to the redshift of the CTS absorption as the O/P ratio increases. Figure 4(a) shows the refractive index dispersion of OP*X* glasses. As indicated in Table 3, as the O/P ratio increases, the refractive index increases, and the Abbe number decreases. Here, the Abbe number is defined as $\nu_d = (n_d-1)/(n_F-n_C)$, where n_d, n_F, and n_C are the refractive indices at d (587.56 nm), F (486.1 nm), and C

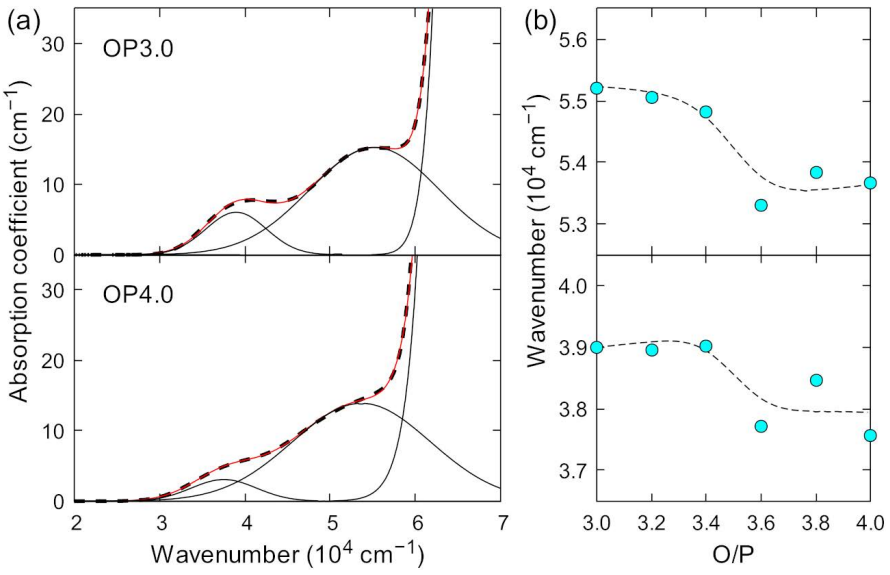

Fig. 3 (a) Spectral deconvolution of the optical absorption spectra for OP3.0 and OP4.0 glasses; (b) relationships between the peak positions and O/P ratio. The dashed and solid lines in (a) are the experimental and fitted data, respectively, and the dashed lines in (b) are guides for the eye.

Table 4 Results of the quantitative analysis of trace impurities by inductively coupled plasma–mass spectrometry (ICP–MS)

	Cr (mg/kg)	Mn (mg/kg)	Fe (mg/kg)	Co (mg/kg)	Ni (mg/kg)	Cu (mg/kg)	Mo (mg/kg)	Pt (mg/kg)
OP3.0	1.3	0.2	21.9	< 0.1	0.3	0.2	< 0.1	0.5
OP3.2	1.0	0.1	16.9	< 0.1	0.2	< 0.1	< 0.1	0.2
OP3.4	1.2	0.1	20.8	< 0.1	0.2	< 0.1	< 0.1	< 0.1
OP3.6	1.3	0.2	21.3	< 0.1	0.2	< 0.1	< 0.1	< 0.1
OP3.8	1.2	0.1	18.7	< 0.1	0.1	< 0.1	< 0.1	< 0.1
OP4.0	1.1	0.1	17.5	< 0.1	0.1	< 0.1	< 0.1	< 0.1

(656.3 nm) lines, respectively. Figure 4(b) shows the correlation between n_d and O/P ratio. It is noted that Fig. 4(b) shows that n_d increases nonlinearly with the O/P ratio: The increase of n_d with respect to the O/P ratio is greater at O/P = 3.6–4.0 than at O/P = 3.0–3.4. The refractive index dispersion is fitted using the Lorentz model, as represented by the following equation:

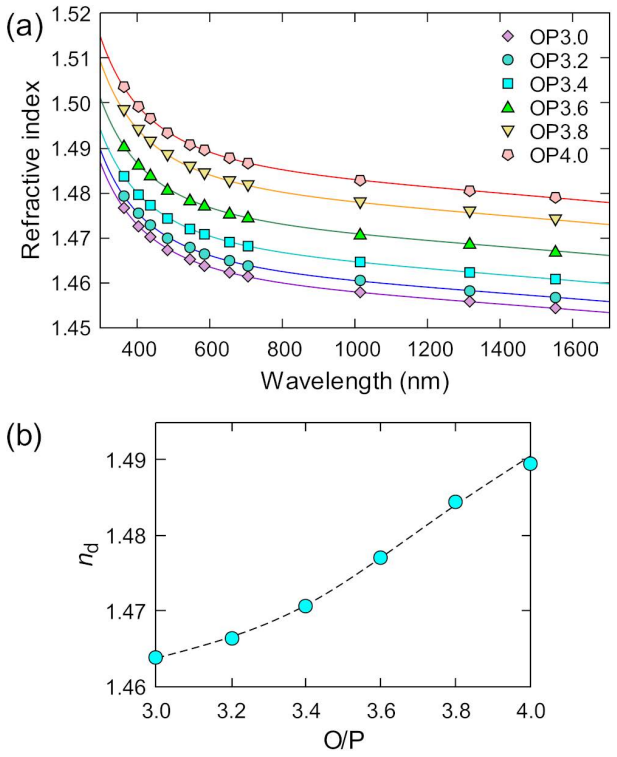

Fig. 4 (a) Refractive index dispersion of OP*X* glasses; (b) O/P dependence of n_d. The solid lines in (a) represent curves fitted using the Lorentz model, and the dashed line in (b) is guide for the eye.

$$(n+jk)^2 = 1+\frac{e^2}{\varepsilon_0 m}\sum_i \frac{N_i}{(\omega_i^2-\omega^2-j\omega\gamma_i)} \quad (2)$$

where n is the refractive index, j is the pure imaginary complex number, k is the extinction coefficient, e is the elementary charge, ε_0 is the electric permittivity of a vacuum, m is the mass of the electron, i is the type of oscillator, N_i is the number density of the oscillator, ω is the angular frequency, ω_i is the resonance frequency, and γ_i is the damping coefficient. Here, k and γ_i are assumed to be zero because the samples are optically transparent at the measured wavelength. Additionally, Eq. (2) can be simplified as the following equation, assuming that there are only two resonance terms in the UV and IR regions:

$$n^2 = 1+\frac{e^2}{\varepsilon_0 m}\left(\frac{N_{UV}}{\omega_{UV}^2-\omega^2}+\frac{N_{IR}}{\omega_{IR}^2-\omega^2}\right) \quad (3)$$

where N_{UV} and N_{IR} are the number densities of oscillators in the UV and IR regions, respectively, and ω_{UV} and ω_{IR} are the resonance frequencies in the UV and IR regions, respectively. As shown in Fig. 4(a), the refractive index dispersion of OP*X* glasses can be well represented by the two-term Lorentz model given in Eq. (3).

Figure 5 shows the O/P ratio dependence of the fitting

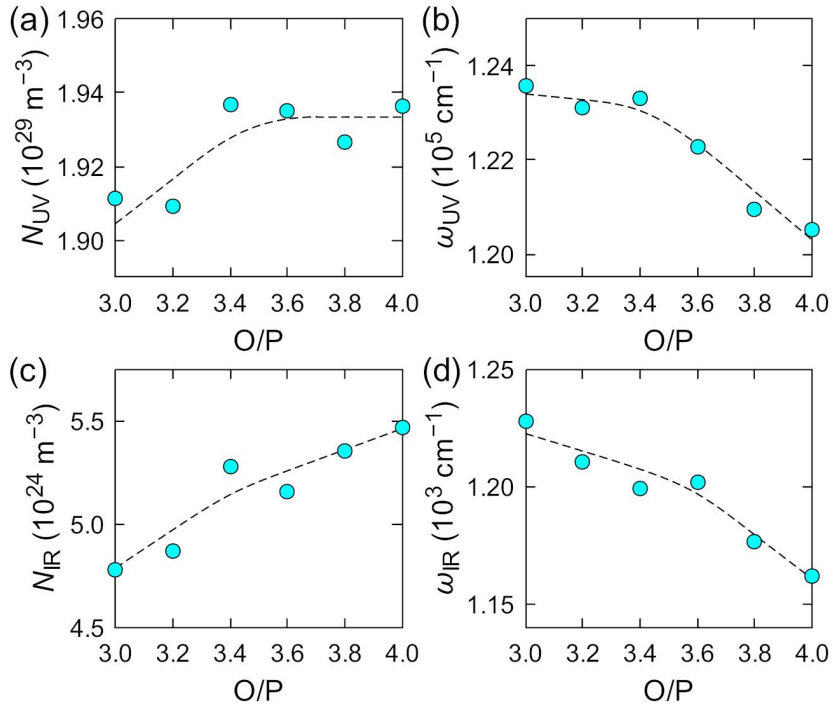

Fig. 5 Dispersion parameters of the OP*X* glasses: (a) N_{UV}, (b) ω_{UV}, (c) N_{IR}, and (d) ω_{IR}. The dashed lines are guides for the eye.

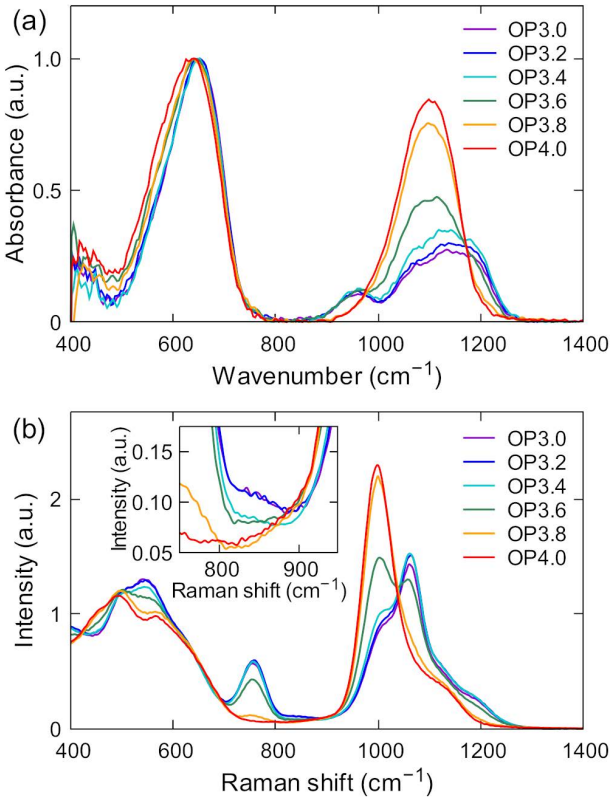

Fig. 6 (a) Infrared (IR) absorption and (b) Raman scattering spectra of the OP*X* glasses. The inset in (b) shows an enlarged view.

parameters determined using Eq. (3). As O/P increases, N_{UV} seems to increase from O/P = 3.0 to 3.4 but remains almost constant at O/P = 3.6–4.0 (Fig. 5(a)). On the other hand, ω_{UV} shifts to lower wave numbers as the O/P ratio increases, and the slope becomes considerably larger at O/P = 3.6–4.0 than that at O/P = 3.0–3.4 (Fig. 5(b)). The dependence of ω_{UV} on the O/P ratio is consistent with the compositional change of E_g presented in Table 3 and Fig. 2. The above results indicate that the increase in the refractive index with the increase in the O/P ratio at O/P = 3.0–3.4 and O/P = 3.6–4.0 is mainly due to the increase in N_{UV} and the shift in ω_{UV}, respectively. As for the oscillator parameters in IR region, with an increase in the O/P ratio, N_{IR} increases almost monotonically, and ω_{IR} shifts to lower wave numbers, but the slope of ω_{IR} at O/P = 3.6–4.0 is slightly larger than that at O/P = 3.0–3.4. Therefore, the compositional dependence of the dispersion parameters in the UV and IR regions is considered to reflect changes in the electronic states and network structures of the OP*X* glasses, respectively.

Figure 6(a) shows the IR absorption spectra of the OP*X* glasses. There is no significant change in the spectrum at O/P = 3.0–3.4; however, at O/P = 3.6–4.0, the peak at 650 cm^{-1} shifts to a slightly lower wave number with an increase in the O/P ratio. In addition, the intensities at 950 and 1200 cm^{-1} decrease, whereas those at 1100 cm^{-1} increase. Because the spectrum in the range of 800–1250 cm^{-1} is attributed to the structure of the phosphate units, these changes in the spectrum at O/P = 3.6–4.0 reflect a drastic structural change in the phosphate groups that form the glass network. As shown in Fig. 7(a), the IR absorption spectrum at 800–1250 cm^{-1} can be deconvoluted into four Gaussian functions. Band A (1150–1190 cm^{-1}) corresponds to asymmetric stretching (ν_{as}) of P–O bonds in $P\emptyset_2O_2^-$ (Q^2) units [10], [13], [19], band B (1130 cm^{-1}) is ν_{as} of P–O bonds in $P\emptyset O_3^{2-}$ (Q^1) units [10], [13], [19], [20], band C (1080 cm^{-1}) is the symmetric stretching (ν_s) of P–O bonds in $P\emptyset O_3^{2-}$ (Q^1) units and ν_{as} of P–O bonds in PO_4^{3-} (Q^0) units [10], [13], [19] and band D (960 cm^{-1}) is ν_{as} of P–O–P bonds [10], [19], [20]. Here, Ø is bridging oxygen. The absence of a band at 1350 cm^{-1} assigned to ν_s of P = O double bonds in $P\emptyset_3O$ (Q^3) units [14] indicates that the fraction of Q^3 units is very small in the OP*X* glasses. As shown in Fig. 7(a), the peak position of band A (ν_{as} P–O in Q^2) is located at 1189 cm^{-1} in the OP3.0 glass and 1156 cm^{-1} in OP4.0 glass, showing a shift to a lower wave number as the O/P ratio increases. This suggests a decrease in the length of the phosphate chains containing Q^2 units with increasing O/P ratio [21]. The fraction of each peak area in Fig. 7(a) is shown in part (b). The fractions of bands A (ν_{as} P–O in Q^2) and D (ν_{as} P–O–P) are largely constant at O/P = 3.0–3.4; however, at O/P = 3.6–4.0, they decrease monotonically as the O/P ratio increases. On the other hand, the fraction of band C (ν_s P–O in Q^1, ν_{as} P–O in Q^0) increases with the increase in the O/P ratio from 3.6 to 4.0. The fraction of band B (ν_{as} P–O in Q^1) does not show a clear dependence on the O/P ratio.

Figure 6(b) shows the Raman scattering spectra of the OP*X* glasses. Similar to the IR absorption spectra, no significant change is observed in the Raman spectra at O/P = 3.0–3.4; however, with an increase in the O/P ratio from 3.6 to 4.0, the intensities at 540, 750, 1060, and 1200 cm^{-1} decrease, whereas those at 460 and 1000 cm^{-1} increase. Figure 7(c) shows the result of spectral deconvolution of the Raman spectra at 800–1250 cm^{-1} using four Gaussian functions. Band E (1160–1180 cm^{-1}) is ν_s of P–O bonds in $P\emptyset_2O_2^-$ (Q^2) units [6], [10], [13], [19], [22], band F (1110 cm^{-1}) is ν_{as} of P–O bonds in $P\emptyset O_3^{2-}$ (Q^1) units [6], [10], [22], band G (1050 cm^{-1}) is ν_s of P–O bonds in $P\emptyset O_3^{2-}$ (Q^1) units [10], [13], [19], [22] and pyrophosphate $P_2O_7^{4-}$ groups [19], and band H (1000–1020 cm^{-1}) is ν_s of P–O bonds in PO_4^{3-} (Q^0) units [6], [10], [13], [19], [22]. The fraction of each peak area in Fig. 7(c) is shown in Fig. 7(d). The ratio of each peak area is almost constant at O/P = 3.0–3.4; however, at O/P = 3.6–4.0, the fractions of bands E (ν_s P–O in

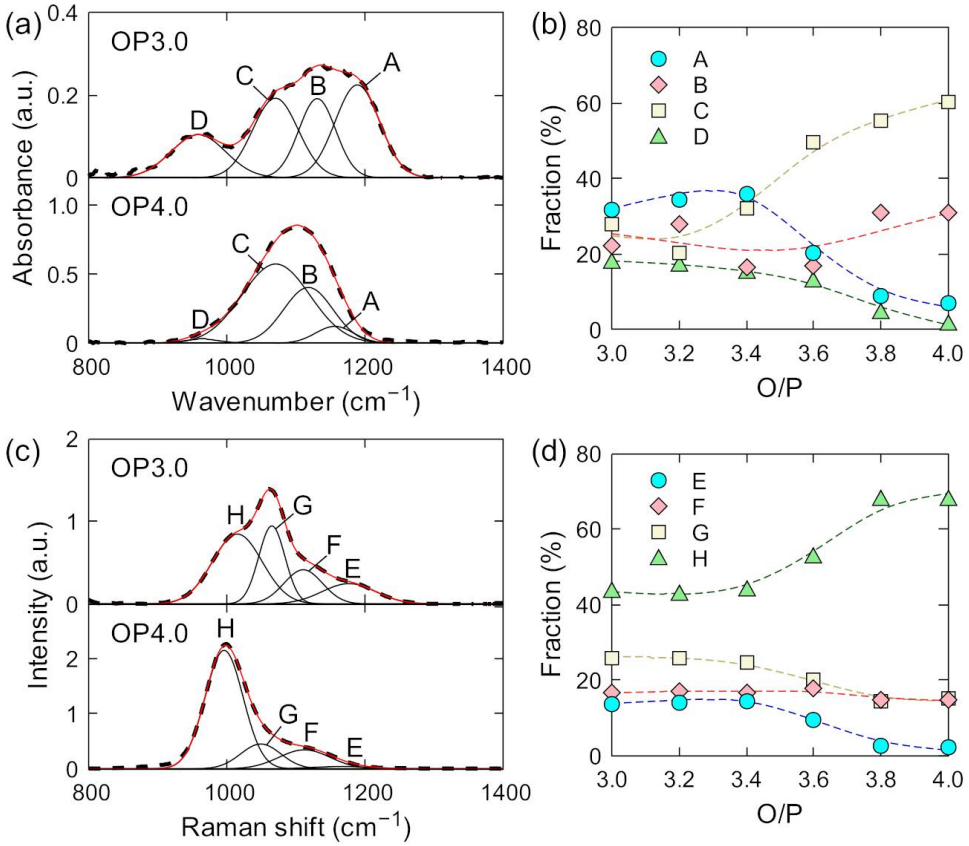

Fig. 7 Spectral deconvolution of (a) infrared (IR) absorption and (c) Raman scattering spectra for the OP3.0 and OP4.0 glasses, and the fraction of each peak area in the (b) infrared (IR) absorption and (d) Raman scattering spectra. The dashed and solid lines in (a, c) are the experimental and fitted data, respectively, and the dashed lines in (b, d) are guides for the eye.

Table 5 Assignments of infrared (IR) and Raman bands attributed to phosphate units in OP*X* glasses

IR				Raman			
Band	Wavenumber (cm^{-1})	Assignment	Ref.	Band	Wavenumber (cm^{-1})	Assignment	Ref.
A	1090–1150	ν_{as} P–O in Q^2	[10], [13], [19]	E	1160–1180	ν_s P–O in Q^2	[6], [10], [13], [19], [22]
B	~1130	ν_{as} P–O in Q^1	[10], [13], [19], [20]	F	~1100	ν_{as} P–O in Q^1	[6], [10], [22]
C	~1080	ν_s P–O in Q^1	[10], [13], [19]	G	~1050	ν_s P–O in Q^1	[10], [13], [19], [22]
		ν_{as} P–O in Q^0	[10], [13], [19]			ν_s $P_2O_7^{4-}$	[19]
D	~960	ν_{as} P–O–P	[10], [19], [20]	H	1000–1020	ν_s P–O in Q^0	[6], [10], [13], [19], [22]

Q^2) and G (ν_s P–O in Q^1, ν_s $P_2O_7^{4-}$) decrease, and that of band H (ν_s P–O in Q^0) increase as the O/P ratio increases. On the other hand, band F shows an almost constant fraction regardless of the O/P ratio. The assignments of IR and Raman bands attributed to phosphate units in OP*X* glasses are summarized in Table 5.

The results in Fig. 7 strongly indicate a structural change of Q^2 units to Q^0 units with an increase in the O/P ratio at O/P = 3.6–4.0. The Raman spectra additionally support the breakage of the phosphate chains with increasing O/P ratio because the band at 750 cm^{-1}, which is assigned to the symmetric stretching mode of P–O–P bonds in the phosphate chains [6], [10], [19], [22], decreases in intensity with the O/P ratio at O/P = 3.6–4.0 (Fig. 6(b)). In addition, a slight band is confirmed at 850 cm^{-1} in the Raman spectra (inset of Fig. 6(b)), and its intensity decreases as the O/P ratio increases, almost disappearing at O/P = 3.6–4.0. Because this band is attributed to the symmetric stretching of F–P–F bonds [6], [23], it indicates that P–F bonds are present at low O/P ratios. The symmetric stretching vibration of P–F bond is reported to appear around 760 cm^{-1} [6], [13], [23], but it is difficult to evaluate it independently because it overlaps with the peak of the symmetric stretching vibration of P–O–P (750 cm^{-1}).

The evaluation of the low-frequency region (< 700 cm^{-1}) in the IR and Raman spectra of OP*X* glasses is more complicated. In aluminofluoride–phosphate systems, various modes due to the Al–(O, F) and P–(O, F) networks overlap in this region, and their frequencies also depend on the degree of polymerization [24]. The IR bands due to the vibrations of AlO_6, AlO_4, AlF_6, and AlF_4 appear at 535, 730, 540–570, and 620 cm^{-1}, respectively [25], and the asymmetric stretching modes of the Al–F–Al groups appear at 630 and 680 cm^{-1} [13]. Furthermore, in the IR absorption spectra, the bending vibrations of O–P–O units and $\delta(PO_2^-)$ modes of $(PO_2^-)_n$ chains show a band at approximately 480 cm^{-1}, and the band at 540 cm^{-1} is described as a fundamental frequency of Q^0 units or as harmonics of P = O bending vibrations [20]. In Raman spectroscopy, the vibrations of AlF_6 and AlF_4 units appear at 570 and 625 cm^{-1}, respectively [13], and the vibrations of $F_3Al–O–AlF_3$ groups appear at 530 cm^{-1} [13]. In addition, the bending mode of O–P–O in Q^0 units, bending mode of phosphate chains, and symmetric stretching mode of P–O–P bonds in Q^2 units show Raman bands at approximately 440, 560, and 620 cm^{-1}, respectively [19]. From the above, the shift of the IR absorption peak at 650 cm^{-1} with an increase in the O/P ratio (Fig. 6(a)) may reflect structural changes, such as a decrease in P–F bonds, an increase in Q^0 units, and a transformation from AlF_6 and AlF_4 to $Al(O, F)_6$. In addition, the decrease in intensity at 550 cm^{-1} and increase at 480 cm^{-1} in the Raman spectra (Fig. 6(b)) possibly reflect the structural changes of phosphate groups, such as the increase in Q^0 units and breakage of the phosphate chains with the increase in the O/P ratio.

4 Discussion

The IR and Raman spectroscopy results strongly indicate that the increase in the O/P ratio from 3.6 to 4.0 leads to the breakage of the phosphate chains, causing a decrease in Q^2 units and an increase in isolated Q^0 units. The increase in N_{IR} and decrease in ω_{IR} with increasing O/P ratio (Figs. 5(c, d)) are also consistent with the spectral changes caused by the decrease in Q^2 units and increase in Q^0 units (Fig. 6(a)). This nonlinear structural change with the variation in the O/P ratio can be understood by considering the structure of phosphate glass, which is well described using the O/P ratio [14]. At O/P = 3.0–3.5, metaphosphate groups $[(PO_3)_n]$ are obtained, and the structure can be described as chains formed by PO_4 tetrahedra. In contrast, when the O/P ratio is between 3.5 and 4.0, isolated orthophosphate units (PO_4^{3-}) are generated. It should be noted that these orthophosphate units are separated from other $P(O, F)_4$ tetrahedra but are expected to be linked to Al–(O, F) polyhedra because previous structural analyses of fluoride–phosphate glass have shown that $Al(O, F)_6$ octahedra interconnect with phosphate monomers and dimers [26], [27]. In this study, however, oxygens in P–O–Al bonds are classified as non-bridging oxygens because the differences in electronegativities between Al (1.61) and O (3.44) are significantly larger than that between P (2.19) and O (3.44), resulting in more the ionicity of Al–O bonds than P–O bonds [28].

Although OP*X* glasses have a much lower oxygen content than fluorine content, structures in phosphate groups are strongly dependent on the O/P ratio, similar to phosphate glass. Therefore, it is suggested that P preferentially coordinates with oxygen, and this is also supported by the fact that the Raman intensity of F–P–F bonds is very weak compared with that of P–O-related bands (Fig. 6(b)). Such selectivity has also been reported in oxyfluoroborate glass, and its origin was discussed using the concept of electronegativity by Shinozaki et al [29]. The Pauling electronegativity values are Ba (0.89) < Ca (1.00) < Al (1.61) < P (2.19) < O (3.44) < F (3.98) [28]. Ba and Ca, which have low electronegativities, strongly attract fluorine and preferentially form ionic bonds. In contrast, P, which has a higher electronegativity than other cations, is more likely to form covalent bonds with oxygen, which has a more similar electronegativity than fluorine.

From the results of IR and Raman spectroscopy, almost no structural change was observed at O/P = 3.0–3.4, but significant structural changes were confirmed at O/P = 3.6–4.0. One possible explanation for this nonlinear trend is the effect of P–F bonds. Although the intensity of the Raman peak is small, Fig. 6(b) suggests the presence of F–P–F bonds at O/P = 3.0–3.4, and its intensity decreases with the increase of O/P ratio. Therefore, at O/P = 3.0–3.4, it is suggested that terminal fluorines in P–F bonds are replaced by oxygen as the O/P ratio increases. According to Ref. [26], fluorine preferentially replaces bridging oxygen on the phosphate tetrahedra [26]. If so, when the O/P ratio increases at O/P = 3.0–3.4, the introduced oxygen is expected to preferentially replace the fluorine in the P–F bonds to form the bridging P–O–P bonds. From Fig. 7, it can be seen that the fraction of IR band A (ν_{as} P–O in Q^2) and Raman band E (ν_s P–O in Q^2) slightly increase with O/P ratio at O/P = 3.0–3.4, supporting the formation of bridging P–O–P bonds by F → O substitution. Similarly, it is also expected that IR band D (ν_{as} P–O–P) and Raman band at 750 cm^{-1} (ν_s P–O–P) increase with O/P ratio at O/P = 3.0–3.4, but the results

do not show a clear increase. This might be due to the overlap of these bands with vibrational components originating from the fluorophosphate units because it has been reported that the F–P–F and P–F bonds exhibit vibrational peaks at 980 cm^{-1} in IR spectra [11], [25], and 760 cm^{-1} in Raman spectra [6], [13], [23], respectively. At O/P = 3.0–3.4, the fraction and peak intensity in vibrational spectra of these fluorophosphate units should decrease with increasing O/P ratio.

According to the previous study [13], [23], the vibrational energy of non-bridging oxygen connected with P in $P(O, F)_4$ strongly depends on the number of non-bridging oxygens. This is because the bond order of terminal oxygen is averaged over the total number of non-bridging oxygens, so $PØO_2F^-$, $PO_2F_2^-$, and $PØ_2O_2^-$ (Q^2) units have almost the same bond order of 1.5 between P and the terminal oxygen atoms. Similarly, less polymerized PO_3F^{2-} and $PØO_3^{2-}$ (Q^1) units would have almost the same bond order as 1.33. Therefore, even if the terminal fluorines in the P–F bonds are replaced with bridging oxygens at O/P = 3.0–3.4, it is estimated that the vibrational energy is hardly changed. At O/P=3.6–4.0, on the other hand, there should be almost no P–F bonds remaining due to the substitution to P–O–P bonds, so the oxygens introduced by increasing the O/P ratio preferentially form $P–O^-$ and P–O–Al bonds, leading the drastic structural change of phosphate units ($Q^2 \rightarrow Q^0$).

Finally, we discuss the relationship between the structural changes in the OP*X* glasses and their optical properties. Using the concept of optical basicity proposed by Duffy and Ingram, the optical basicities of the Q^2, Q^1, and Q^0 units are 0.50, 0.57, and 0.63, respectively [30]. This indicates that the electron-donating ability of oxygen increases as the number of non-bridging oxygen atoms in the PO_4 tetrahedron increases. This is because non-bridging oxygen generally has a smaller binding energy of outer electrons than bridging oxygen, resulting in a higher energy level of the O 2p orbital, which forms the upper valence states of the glass [31], [32]. In the OP*X* glasses, it is strongly expected that the energy level of the O 2p orbital shifts to a higher energy owing to the non-bridging oxygen generated with the increase in the O/P ratio at 3.6–4.0. The high-energy shift of the O 2p level reduces the transition energy to the conduction band, resulting in a decrease in the bandgap energy, as indicated in Table 3 and Fig. 2. This mechanism is also important for the refractive index dispersion because the redshift of the intrinsic resonance frequency, ω_{UV}, can be explained in the same manner. As for the CTS transition band, the relationship between the electron-donating ability of ligand anions and the CTS transition energy has been discussed in other studies [18], [33]. Considering this, the nonlinear decrease in the CTS transition energy from O 2p to Fe^{3+} 3d (Fig. 3) can also be explained by the drastic increase in the electron-donating ability of oxygen by the generation of non-bridging oxygen at O/P = 3.6–4.0. As for the refractive index, Fig. 4(b) clearly shows that the increase of n_d with respect to the O/P ratio is greater at O/P = 3.6–4.0 than at O/P = 3.0–3.4. At O/P = 3.0–3.4, it is estimated that n_d increases simply due to the increase in the number density of oxide ions with higher polarizability than fluoride ions because there is no significant change in the Q^n distribution. On the other hand, at O/P = 3.6–4.0, in addition to the effect of an increase in the number density of oxide ions, the increase in optical basicity (number density of non-bridging oxygens) caused by a drastic change in the Q^n distribution should contribute to increase n_d.

5 Conclusion

$Ca(PO_3)_2$–AlF_3–CaF_2–BaF_2–BaO glasses were prepared using the melt-quenching method, and the effects of the O/P ratio on the absorption spectrum and refractive index dispersion were evaluated. The bandgap energy determined from the intrinsic interband absorption edge was almost constant at approximately 7.0 eV at O/P = 3.0–3.4, but it rapidly decreased to 6.77 eV with the increase of O/P ratio at 3.6–4.0. Furthermore, the glass contained approximately 20 mg/kg Fe ions, and absorption peaks due to CTS from O 2p to Fe^{3+} 3d were observed at approximately 180 and 260 nm; their peak positions also showed a redshift as the O/P ratio increased from 3.6 to 4.0. We also investigated the refractive index dispersion of the glass using the Lorentz model and clarified the nonlinear O/P dependence of refractive index n_d, the number density of oscillators, and resonance frequencies. IR and Raman spectroscopy suggested that, at O/P = 3.0–3.4, P–F bonds were substituted by bridging P–O–P bonds with an increase of O/P ratio, whereas at O/P = 3.6–4.0, the Q^2 units drastically decreased, and Q^0 units were generated as the O/P ratio increased, indicating the breakage of phosphate chains in the glass. From these results, it was concluded that the nonlinear changes in the optical properties with respect to the O/P ratio were due to an increase in non-bridging oxygen associated with the breakage of the phosphate chains: The increase in non-bridging oxygen with a high electron-donating ability enhanced the energy level of the upper valence band, resulting in a decrease in the transition energies from the O 2p level to the conduction band and

Fe^{3+} 3d level.

Acknowledgment. The authors acknowledge M. Fujiwara (Nikon Corp.) and I. Sato (Nikon Corp.) for their help with the ICP–MS analysis and K. Kato (Nikon Corp.) for their assistance with the VUV measurements.

References

[1] D. Ehrt and W. Seeber, "Glass for high performance optics and laser technology," *Journal of Non-Crystalline Solids,* vol. 129, no. 1–3, pp. 19–30, 1991.

[2] D. Ehrt, M. Carl, T. Kittel, M. Müller, and W. Seeber, "High-performance glass for the deep ultraviolet range," *Journal of Non-Crystalline Solids,* vol. 177, pp. 405–419, 1994.

[3] R. Lebullenger, L. A. O. Nunes, and A. C. Hernandes, "Properties of glasses from fluoride to phosphate composition," *Journal of Non-Crystalline Solids,* vol. 284, no. 1–3, pp. 55–60, 2001.

[4] D. Ehrt, "Phosphate and fluoride phosphate optical glasses—properties, structure and applications," *Physics and Chemistry of Glasses-European Journal of Glass Science and Technology Part B,* vol. 56, no. 6, pp. 217–234, 2015.

[5] W. Jahn, "Mehrstoffsysteme zum aufbau optischer gläser," *Glastechnische Berichte,* vol. 34, pp. 107–120, 1961.

[6] J. J. Videau, J. Portier, and B. Piriou, "Raman spectroscopic studies of fluorophosphate glasses," *Journal of Non-Crystalline Solids*, vol. 48, no. 2, pp. 385–392, 1982.

[7] U. Bärenwald, M. Dubiel, W. Matz, and D. Ehrt, "Structural models of the fluoroaluminate glass system $Ba(PO_3)_2$–CaF_2–AlF_3," *Journal of Non-Crystalline Solids,* vol. 130, no. 2, pp. 171–181, 1991.

[8] L. F. Santos, M. Almeida R, V. K. Tikhomirov, and A. Jha, "Raman spectra and structure of fluoroaluminophosphate glasses," *Journal of Non-Crystalline Solids*, vol. 284, no. 1–3, pp. 43–48, 2001.

[9] M. Nalin, S. J. L. Ribeiro, Y. Messaddeq, J. Schneider, and P. Donoso, "Scandium fluorophosphate glasses: a structural approach," *Comptes Rendus Chimie,* vol. 5, no. 12, pp. 915–920, 2002.

[10] D. Möncke, D. Ehrt, L. L. Velli, C. P. E. Varsamis, and E. I. Kamitsos, "Structural investigations of fluoride phosphate glasses," *Proceedings of XX International Congress on Glass,* Vols. P-10–030, pp. 1–6, 2004.

[11] H. Sun, L. Zhang, S. Xu, S. Dai, J. Zhang, L. Hu, and Z. Jiang, "Structure and thermal stability of novel fluorophosphate glasses," *Journal of Alloys and Compounds,* vol. 391, no. 1–2, pp. 151–155, 2005.

[12] D. Möncke, D. Ehrt, L. L. Velli, C. P. E. Varsamis, E. I. Kamitsos, S. Elbers, and H. Eckert, "Comparative spectroscopic investigation of different types of fluoride phosphate glasses," *Physics and Chemistry of Glasses - European Journal of Glass Science and Technology Part B*, vol. 48, no. 6, pp. 399–402, 2007.

[13] D. Möncke and H. Eckert, "Review on the structural analysis of fluoride-phosphate and fluorophosphate glasses," *Journal of Non-Crystalline Solids: X*, vol. 3, 100026, 2019.

[14] R. K. Brow, "Review: the structure of simple phosphate glasses," *Journal of Non-Crystalline Solids,* Vols. 263–264, no. 1, pp. 1–28, 2000.

[15] F. A. Santos, J. R. J. Delben, A. A. S. T. Delben, L. H. C. Andrade, and S. M. Lima, "Thermal stability and crystallization behavior of TiO_2 doped ZBLAN glasses," *Journal of Non-Crystalline Solids,* vol. 357, no. 15, pp. 2907–2910, 2011.

[16] M. Çelikbilek, A. E. Ersundu, and S. Aydin, "Preparation and characterization of TeO_2–WO_3–Li_2O glasses," *Journal of Non-Crystalline Solids,* vol. 378, pp. 247–253, 2013.

[17] L. Liu, C. Liu, X. Wang, Z. G. Hu, R. K. Li, and C. T. Chen, "Impact of Fe^{3+} on UV absorption of $K_2Al_2B_2O_7$ crystals," *Solid state sciences,* vol. 11, no. 4, pp. 841–844, 2009.

[18] D. Möncke and D. Ehrt, "Charge transfer transitions in glasses - Attempt of a systematic review," *Optical Materials: X,* vol. 12, 100092, 2021.

[19] A. Moguš-Milanković, A. Šantić, S. T. Reis, K. Furić, and D. E. Day, "Mixed ion–polaron transport in Na_2O–PbO–Fe_2O_3–P_2O_5 glasses," *Journal of Non-Crystalline Solids,* vol. 342, no. 1–3, pp. 97–109, 2004.

[20] C. Ivascu, A. T. Gabor, O. Cozar, L. Daraban, and I. Ardelean, "FT-IR, Raman and thermoluminescence investigation of P_2O_5–BaO–Li_2O glass system," *Journal of Molecular Structure,* vol. 993, no. 1–3, pp. 249–253, 2011.

[21] L. Koudelka, J. Klikorka, M. Frumar, M. Pisárčik, V. Kellö, V. D. Khalilev, V. I. Vakhrameev, and G. D. Chkhenkeli, "Raman spectra and structure of fluorophosphate glasses of $(1-x)Ba(PO_3)_2$–$x$$LiRAlF_6$," *Journal of Non-Crystalline Solids,* vol. 85, no. 1–2, pp. 204–210, 1986.

[22] R. K. Brow, D. R. Tallant, S. T. Myers, and C. C. Phifer, "The short-range structure of zinc polyphosphate glass," *Journal of Non-Crystalline Solids,* vol. 191, no. 1–2, pp. 45–55, 1995.

[23] V. K. Bühler and W. Bues, "Schwingungsspektren von fluot-ophosphatschmelzen und -kristallea," *Zeitschrift für anorganische und allgemeine Chemie,* vol. 308, pp. 62–71, 1961.

[24] P. Tarte, "Infra-red spectra of inorganic aluminates and characteristic vibrational frequencies of AlO_4 tetrahedra and AlO_6 octahedra," *Spectrochimica Acta Part A: Molecular Spectroscopy,* vol. 23, no. 7, pp. 2127–2143, 1967.

[25] B. Karmakar, P. Kundu, and R. N. Dwivedi, "IR spectra and

their application for evaluating physical properties of fluorophosphate glasses," *Journal of Non-Crystalline Solids,* vol. 289, no. 1–3, pp. 155–162, 2001.

[26] R. K. Brow, Z. A. Osborne, and R. J. Kirkpatrick, "A multinuclear MAS NMR study of the short-range structure of fluorophosphate glass," *Journal of Materials Research*, vol. 7, no. 7, pp. 1892–1899, 1992.

[27] D. Ehrt, "Structure and properties of fluoride phosphate glasses," *Proceedings SPIE*, vol. 1761, pp. 213–222, 1992.

[28] L. Pauling, "The nature of the chemical bond. IV. The energy of single bonds and the relative electronegativity of atoms," *Journal of the American Chemical Society,* vol. 54, no. 9, pp. 3570–3582, 1932.

[29] K. Shinozaki, S. Sukenaga, and K. Ohara, "Photoluminescence and structural similarity of crystals with oxide–fluoride stacking structure and oxyfluoride glass," *Journal of the Ceramic Society of Japan,* vol. 128, no. 12, pp. 1030–1037, 2020.

[30] J. A. Duffy and M. D. Ingram, "An interpretation of glass chemistry in terms of the optical basicity concept," *Journal of Non-Crystalline Solids,* vol. 21, no. 3, pp. 373–410, 1976.

[31] S. K. J. Al-Ani, C. A. Hogarth, and R. A. El-Malawany, "A study of optical absorption in tellurite and tungsten-tellurite glasses," *Journal of materials science,* vol. 20, pp. 661–667, 1985.

[32] B. S. Bae and M. C. Weinberg, "Ultraviolet optical absorptions of semiconducting copper phosphate glasses," *Journal of Applied physics,* vol. 73, no. 11, pp. 7760–7766, 1993.

[33] J. A. Duffy, "Charge transfer spectra of metal ions in glass," *Physics and Chemistry of Glasses,* vol. 38, no. 6, pp. 289–292, 1997.

[34] K. Yoshimoto, M. Ueda, Y. Yamamoto, and M. Mizuguchi, "Impact of the O/P ratio on the optical properties and structures of fluoride–phosphate glass," *Journal of the American Ceramic Society*, vol. 106, no. 5, pp. 2852–2861, 2023.

吉本幸平　Kohei YOSHIMOTO
生産本部 技術統括部 光学素材部
Optical Material Department
Technology Sector
Production Technology Division

上田　基　Motoi UEDA
先進技術開発本部
Advanced Technology Research & Development Division

山本優也　Yuya YAMAMOTO
先進技術開発本部 材料・要素技術研究所
Materials & Advanced Research Laboratory
Advanced Technology Research & Development Division

水口雅史　Masafumi MIZUGUCHI
先進技術開発本部 材料・要素技術研究所
Materials & Advanced Research Laboratory
Advanced Technology Research & Development Division


吉本幸平
Kohei YOSHIMOTO


上田　基
Motoi UEDA


山本優也
Yuya YAMAMOTO


水口雅史
Masafumi MIZUGUCHI